

Variational Optimization for Quantum Problems using Deep Generative Networks

Lingxia Zhang,^{1,*} Xiaodie Lin,^{2,*} Peidong Wang,¹ Kaiyan Yang,¹ Xiao Zeng,¹ Zhaohui Wei,^{3,4,†} and Zizhu Wang^{1,‡}

¹*Institute of Fundamental and Frontier Sciences and Ministry of Education Key Laboratory of Quantum Physics and Photonic Quantum Information, University of Electronic Science and Technology of China, Chengdu 611731, China*

²*Institute for Interdisciplinary Information Sciences, Tsinghua University, Beijing 100084, China*

³*Yau Mathematical Sciences Center, Tsinghua University, Beijing 100084, China*

⁴*Yanqi Lake Beijing Institute of Mathematical Sciences and Applications, Beijing 101407, China*

Optimization is one of the keystones of modern science and engineering. Its applications in quantum technology and machine learning helped nurture variational quantum algorithms and generative AI respectively. We propose a general approach to design variational optimization algorithms based on generative models: the Variational Generative Optimization Network (VGON). To demonstrate its broad applicability, we apply VGON to three quantum tasks: finding the best state in an entanglement-detection protocol, finding the ground state of a 1D quantum spin model with variational quantum circuits, and generating degenerate ground states of many-body quantum Hamiltonians. For the first task, VGON greatly reduces the optimization time compared to stochastic gradient descent while generating nearly optimal quantum states. For the second task, VGON alleviates the barren plateau problem in variational quantum circuits. For the final task, VGON can identify the degenerate ground state spaces after a single stage of training and generate a variety of states therein.

CONTENTS

I. Introduction	1	D. Identifying degenerate ground state space of quantum models	15
II. The VGON model	2	1. The Majumdar-Ghosh model	15
III. Finding the optimal state for entanglement detection	3	2. The 232 model	16
IV. Alleviating the effect of barren plateaux in variational quantum algorithms	4	I. INTRODUCTION	
V. Identifying degenerate ground state space of quantum models	5	Mathematical optimization is ubiquitous in modern science and technology. Spanning diverse fields like economics, chemistry, physics, and various engineering areas, its applications abound (Kochenderfer and Wheeler, 2019). In quantum information theory, many problems relating to the approximation and characterization of quantum correlations can be formulated as convex optimization (Boyd and Vandenberghe, 2004) problems, which is a particular kind of mathematical optimization with provable global optimality guarantees. Typical examples include the Doherty-Parrilo-Spedalieri (DPS) hierarchy (Doherty <i>et al.</i> , 2002) for entanglement certification and the Navascués-Pironio-Acín (NPA) hierarchy (Navascués <i>et al.</i> , 2007; Tavakoli <i>et al.</i> , 2023) for bounding the set of quantum correlations, both relying on finding a hierarchy of semidefinite programming (SDP) relaxations of the original problems which converge to their optimal solutions.	
VI. Conclusions	6	For quantum problems where convexity is hard to come by or the global optimality of the solution is a secondary consideration when compared to the efficiency of the algo-	
References	6		
A. Reaching the quantum limit of a many-body contextuality witness	9		
B. Finding the optimal state for entanglement detection	9		
1. The pure state case	10		
2. The mixed state case	11		
C. Alleviating the effect of barren plateaux in variational quantum algorithms	12		
1. The $Z_1 Z_2$ model	12		
2. The Heisenberg XXZ model	14		

* These authors contributed equally to this work

† weizhaohui@mail.tsinghua.edu.cn

‡ zizhu@uestc.edu.cn

rithm, variational optimization provides a rich toolbox. In quantum many-body simulation, classical variational algorithms based on tensor network states allow the classical descriptions of the ground states of a large class of quantum models to be computed efficiently (Cirac *et al.*, 2021; Haegeman *et al.*, 2011; Milsted *et al.*, 2013; Vanderstraeten *et al.*, 2019; White, 1992). When solutions are expected to be quantum, hybrid quantum-classical variational algorithms are popular choices. Variational optimization is carried out on the classical parameters of these algorithms, while quantum gates and measurements are implemented in the corresponding quantum circuit (Farhi *et al.*, 2014; Havlíček *et al.*, 2019; McArdle *et al.*, 2020; Peruzzo *et al.*, 2014; Romero *et al.*, 2017; Schuld *et al.*, 2020).

Optimization is also at the core of every machine learning algorithm (Murphy, 2022). Generative models, especially the generative pretrained transformer (GPT) (Radford *et al.*, 2017; Vaswani *et al.*, 2017) has opened a new way to address scientific problems that span a broad spectrum. In quantum physics, many-body quantum models can be efficiently solved by a generative model called the restricted Boltzmann machines (Carleo and Troyer, 2017; Melko *et al.*, 2019), lattice gauge theories can be simulated using another generative model called normalizing flows (Li and Wang, 2018; Stornati, 2022), and quantum states can be more efficiently represented by variational autoencoders (VAEs) (Carrasquilla *et al.*, 2019; Kingma and Welling, 2013; Luchnikov *et al.*, 2019; Rocchetto *et al.*, 2018; Sá and Roditi, 2021; van Esbroeck *et al.*, 2020).

However, despite these encouraging advances, current applications of generative models to quantum problems usually focus on learning certain features from training data sets, and then generating new data with similar features. In a quantum problem, the training data may be a quantum state or complex correlation information contained therein, and the neural network is expected to generate new states or information resembling the training set. Extending the possibility of applying generative models to quantum problems beyond this scenario, we envisage using them to find (nearly) optimal solutions to general variational optimization problems.

Here we propose a general approach called the variational generative optimization network (VGON) to fulfill such a task. It contains a pair of classical deep feed-forward neural networks connected by a stochastic latent layer, and a problem-specific objective function. Two essential aspects of the VGON model include its integrated sampling mechanism within the training process and the adaptability of its objective function. The integrated sampling ensures that the outputs can be non-deterministic, which supports the identification of various simultaneous optimal solutions to the objective function. Meanwhile, the adaptable objective function enhances the model’s capacity to extend beyond simple replication of input data, indicating its wide applicability across diverse optimization challenges.

We apply VGON to a variety of quantum problems to

showcase its potential. We first demonstrate that it outperforms stochastic gradient descent (SGD) by avoiding entrapment in local optima in variational optimization problems of modest size, while also converging orders of magnitude faster. For larger problems with tens of thousands of parameters, we show that VGON can substantially alleviate the problem of barren plateaux in parameterized quantum circuits. Since generative models allow multiple optimal solutions to be found and generated simultaneously, a capability that deterministic algorithms lack, we use VGON to explore the ground state space of two quantum many-body models known to be degenerate. We show that VGON can successfully identify the dimension of the ground state space and generate a variety of orthogonal or linearly independent ground states spanning the entire space.

II. THE VGON MODEL

The architecture of VGON, shown in Fig. 1, is similar to that of the variational autoencoder. It consists of two deep feed-forward neural networks, the encoder E_ω and the decoder D_ϕ , connected by a latent layer \mathcal{Z} containing a normal distribution $\mathcal{N}(\boldsymbol{\mu}(z), \boldsymbol{\sigma}^2(z))$, where the mean $\boldsymbol{\mu}$ and the standard deviation $\boldsymbol{\sigma}$ are provided by E_ω . During the training stage, input data \boldsymbol{x}_0 is sampled from a distribution $P(\boldsymbol{x}_0)$, which in all our tests is the uniform distribution over the parameter space. It is then mapped to the latent distribution $\mathcal{N}(\boldsymbol{\mu}(z), \boldsymbol{\sigma}^2(z))$ by the encoder network E_ω . Next the decoder network $D_\phi(z)$ maps data z sampled from the latent distribution $\mathcal{N}(\boldsymbol{\mu}(z), \boldsymbol{\sigma}^2(z))$ to a distribution minimizing the objective function $h(\boldsymbol{x})$. This minimization is achieved by iteratively updating the parameters ω and ϕ in E_ω and D_ϕ , respectively. Due to the existence of a stochastic latent layer, the gradients cannot be propagated backwards in the network. We solve this issue by using the reparameterization trick (Kingma and Welling, 2013).

The key difference between VGON and VAE lies in the objective function (also called the loss function in the machine learning literature): instead of asking the output data distribution to approximate the input distribution by minimizing the Kullback-Leibler (KL) divergence between them, VGON simply requires the output data to minimize any objective function that is appropriate for the target problem. The decoder network, a versatile function approximator, maps the probability distribution from latent space to an output data distribution which can minimize the objective function with high probability (Devroye, 1986; Doersch, 2021). In addition, the KL divergence between the latent distribution $\mathcal{N}(\boldsymbol{\mu}(z), \boldsymbol{\sigma}^2(z))$ and the standard normal distribution $\mathcal{N}(\mathbf{0}, \mathbf{I})$ is also minimized during training, as part of the objective function.

After the objective function converges to within a given tolerance, the training stage is completed. To utilize the trained model, the encoder network is disabled, and data sampled from a standard normal distribution $\mathcal{N}(\mathbf{0}, \mathbf{I})$ are

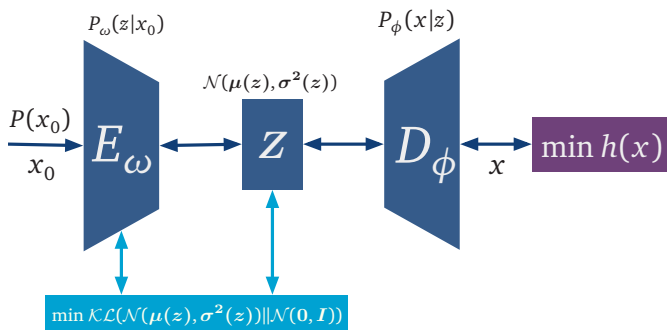


FIG. 1 The framework of VGON. The network is composed of an encoder network E_ω , a latent space Z , and a decoder network D_ϕ . Training data x_0 sampled from $P(x_0)$ is first mapped into a latent distribution $\mathcal{N}(\mu(z), \sigma^2(z))$ by $E_\omega(x_0)$. Then a latent variable z sampled from $\mathcal{N}(\mu(z), \sigma^2(z))$ is transformed to the output x by $D_\phi(z)$. The parameters ϕ and ω are updated iteratively to minimize the objective function $h(x)$.

fed into the decoder network. Depending on the characteristics of the objective function, the corresponding output distribution can be tightly centered around one or multiple optimum values.

To show that VGON can work well, we first use it to solve a variational optimization problem with a known unique optimal solution: finding the minimum ground state energy density among a class of quantum many-body models that matches the lower bound certified by an SDP relaxation. More specifically, we consider a class of infinite 1D translation-invariant (TI) models with fixed couplings discussed in Ref. (Yang *et al.*, 2022), with the optimization variables being the local observables. The ground state energy density of this class of models has a lower bound certified by a variant of the NPA hierarchy (Yang *et al.*, 2022). However, there is no guarantee that any infinite TI quantum many-body Hamiltonian, if couplings are fixed but the dimension of local observables can be arbitrary, can achieve this bound. Meanwhile, by optimizing 3-dimensional local observables with SGD and computing the ground state with uniform matrix product state algorithms (Milsted *et al.*, 2013; Vanderstraeten *et al.*, 2019), a Hamiltonian whose ground state energy density matches the above lower bound to 7 significant digits has been found. We replace SGD with VGON to conduct the same optimization, and find that the converged model can (almost) deterministically generate Hamiltonians whose ground state energy density matches the NPA lower bound to 8 significant digits, reaching the precision limit of commercial SDP solvers (see Appendix A for more technical details). Below we apply VGON to several more complicated problems.

III. FINDING THE OPTIMAL STATE FOR ENTANGLEMENT DETECTION

In a prepare-and-measure entanglement detection game, what is the best state for experimentally demonstrating the advantage of local operations and one-way classical communication (1-LOCC) protocols over protocols using local operations (LO) alone? This problem has practical relevance and does not have a known optimal solution. It can be formulated as a variational optimization problem consisting of multiple convex optimization sub-problems, making it a good showcase of the power of VGON.

Suppose two players, Alice and Bob, receive a bipartite quantum state ρ from a source and want to determine whether ρ is entangled. They have a choice of either performing the experiment in their respective labs, then communicating the outcomes from Alice to Bob thus implementing a 1-LOCC protocol, or forgoing communication completely therefore making the protocol LO. These two scenarios have been formalized as preparation games and introduced in Refs. (Hu *et al.*, 2021; Weilenmann *et al.*, 2021) as a new way of automatically devising experimental protocols to detect quantum entanglement that can minimize the probability of committing statistical errors. Although on certain target quantum states it is possible to show 1-LOCC protocols lead to smaller error probabilities than any LO ones, the advantage is highly dependent on the choice of target states and is hard to analyze.

In this problem, the advantage is defined to be the difference between the minimum probabilities p_2 of committing false-negative statistical errors (a.k.a. type-II errors, defined as a source distributes an entangled state, but Alice and Bob conclude the state they received is separable). It can be computed by solving the following two SDPs and subtracting the two minimal p_2^* corresponding to LO and 1-LOCC protocols:

$$\begin{aligned} \min \quad & p_2 \\ \text{s.t.} \quad & \text{tr}(M_N \rho) = p_2, p_1 \mathbb{I} - M_Y \in \mathcal{S}^*, \\ & M_Y = M_Y(P), M_N = M_N(P), \\ & P \in \mathcal{P}^{\{LO, 1-LOCC\}}. \end{aligned} \quad (1)$$

Here \mathcal{S}^* denotes the dual of the separable set \mathcal{S} . p_1 is the given probability of Alice and Bob making false-positive errors, i.e. type-I error, defined as the scenario in which they conclude that they have received an entangled state, while the source actually distributes a separable one. The positive operator-valued measure (POVM) operators $M_{Y(N)}$ can be constructed as $M_{Y(N)} = \sum_{x,y,a,b} P(x,y,Y(N)|a,b) A_x^a \otimes B_y^b$, where $\{A_x^a\}$ ($\{B_y^b\}$) are predetermined measurements performed by Alice (Bob) with x (y) being measurement labels and a (b) being outcomes. The choice of their protocols is reflected in the sets \mathcal{P}^{LO} or \mathcal{P}^{1-LOCC} in which $P(x,y,Y(N)|a,b)$ is constrained. A more detailed description of the theoretical framework can be found in Appendix B.

For a random quantum state ρ , it turns out that the gap calculated above is usually very small, as shown by the green dots in Figure 2(a). In order to observe the gap under noisy experimental conditions, we would like to know which ρ exhibit the largest gap among the states that can be prepared in a general quantum linear optical setup. Using such a setup as a convenient way to parameterize the state space, we first employ SGD to optimize the gap by starting from random initial pure bipartite qutrit states. The results are shown in Figure 2(a). Because of being trapped easily in local maxima and of needing to compute the gradients with dozens of SDPs, it takes two months to conduct optimizations for 79,663 random initial pure states (see Appendix B.1 for more details). Most of these states exhibit gaps around 0.0036 before optimization, while the largest gap afterwards is 0.083722.

The results of using VGON to solve this problem are depicted in Figure 2(b) and summarized in Table I. Based on 3,000 sets of initial parameters produced by uniform sampling, the model converges after less than two hours of training. After that, we use it to generate 100,000 output states. We find that over 98% of them manifest gaps over 0.08, while over 50% of them have gaps larger than 0.0835. A similar performance has been observed even when choosing the initial quantum states from a variational submanifold of the space of all mixed states, where out of 100,000 states generated by the converged VGON model, 83 have gaps larger than 0.0837, with an average purity of 0.99999 (see Appendix B.2 for more details).

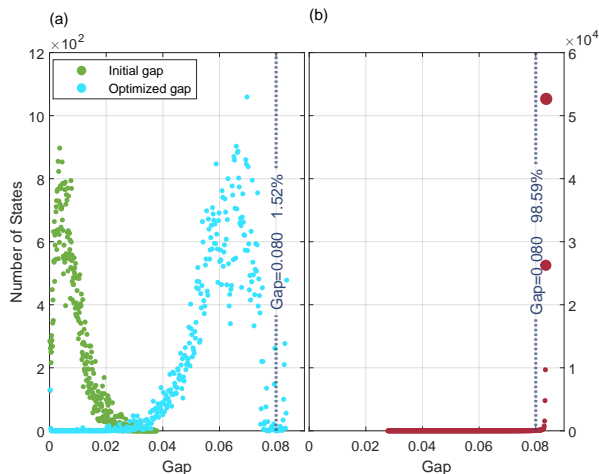


FIG. 2 Comparing SGD and VGON for generating states with large gaps. (a) Most of the 79,663 random initial states for SGD exhibit small gaps around 0.0036, while after optimization most states have gaps smaller than 0.08. The largest gap is 0.083722. (b) Over 98.59% of the 100,000 states generated by a trained VGON model have gaps larger than 0.08, with the largest group, consisting of over 50% of the generated states, tightly centered around 0.0837.

TABLE I Performance comparison between VGON and SGD on finding states maximizing the advantage of 1-LOCC protocols over LO ones.

Method	Percentage of states with gap		
	≥ 0.08	≥ 0.08355	$0.0837 \pm 5 \times 10^{-5}$
SGD pure states	1.52%	0.57%	0.43%
VGON pure states	98.59%	52.75%	9.38%
VGON mixed states	99.32%	57.36%	22.19%

IV. ALLEVIATING THE EFFECT OF BARREN PLATEAUX IN VARIATIONAL QUANTUM ALGORITHMS

On problems with a moderate size of optimization variables, VGON has shown remarkable ability to quickly converge to the (nearly) optimal output distribution and generate high quality solutions with high probability. In near-term hybrid quantum-classical algorithms such as the variational quantum eigensolver (VQE) (Peruzzo *et al.*, 2014), however, the number of classical parameters can quickly reach thousands or tens of thousands. The performance of such a hybrid algorithm can be hard to predict. On the classical part, the problems of vanishing gradients and having multiple minima are often present (Cerezo *et al.*, 2021; Hanin, 2018; Kolen and Kremer, 2001; McClean *et al.*, 2018; Ortiz Marrero *et al.*, 2021). On the quantum part, the choice of ansätze greatly affects the expressivity of the quantum circuit, making the certification of global optimality difficult (Cerezo *et al.*, 2024; Kim *et al.*, 2021; Larocca *et al.*, 2023; Romero *et al.*, 2018; Taube and Bartlett, 2006).

For example, in a typical VQE algorithm, a parameterized variational circuit $U(\theta)$ is used to approximately generate the ground state of a target Hamiltonian H . The circuit structure usually loosely follows the target Hamiltonian and is often called an ansatz. Then by setting the energy of the output state $|\psi(\theta)\rangle = U(\theta)|00\cdots 0\rangle$ with respect to H , i.e., $\langle\psi(\theta)|H|\psi(\theta)\rangle$, as the objective function, the algorithm iteratively updates the parameters in the quantum circuit by applying gradient-based methods on a classical computer. When the algorithm converges, the output quantum state will likely be very close to the ground state of H .

However, when the size of quantum systems increases, gradients vanish exponentially. This is primarily because the random initializations of parameterized unitaries conform to the statistics of a unitary 2-design (Harrow and Low, 2009; McClean *et al.*, 2018), making the working of gradient-based optimization difficult. To overcome the BP problem, several strategies have been proposed and investigated, with the small-angle initialization (VQE-SA) method being identified as an effective technique (Haug *et al.*, 2021; Holmes *et al.*, 2022; Sack *et al.*, 2022). It initializes parameters θ to be close to the zero vector, which differs from the statistics of the parameters from a 2-design and thus may

alleviate the BP problem.

The advantage of VGON over VQE-SA in alleviating BPs can be seen when we use them both, with the same parameterized quantum circuit, to compute the ground state energy of the Heisenberg XXZ model. Its Hamiltonian with periodic boundary conditions is given by

$$H_{XXZ} = - \sum_{i=1}^N (\sigma_x^i \sigma_x^{i+1} + \sigma_y^i \sigma_y^{i+1} - \sigma_z^i \sigma_z^{i+1}),$$

where $\sigma_{x,y,z}^i$ denote the Pauli operators at site i . The ansatz for the parameterized quantum circuit is inspired by the matrix product state encoding (Ran, 2020). It consists of sequential blocks of nearest-neighbor unitary gates, each of which is made of 11 layers of single qubit rotations and CNOT gates (see Appendix C.2 for more details).

By choosing $N = 18$, the circuit contains 816 blocks and 12,240 variational parameters. The average ground state energy, computed using exact diagonalization (ED), is -1.7828. We use both VQE-SA and VGON to compute the same quantity, with each method repeated 10 times. The results are shown in Fig. 3, where the mean values and the 95% confidence intervals of these methods are visualized. The dark-blue and the green lines represent the average energy for VQE-SA and VGON, whose mean values at the last iteration are -1.7613 and -1.7802, respectively. Furthermore, to compare the performance of the two methods in a more fine-grained manner, we also calculate the fidelity between the states produced by the quantum circuit and the exact ground state. As the purple line depicted, VGON can achieve a 99% fidelity by around 880 iterations, while the VQE-SA method can only achieve 78.25% fidelity within the same number of iterations. Moreover, because VGON benefits from batch training, it leads to a more stable convergence. For another comparison, VQE with uniformly random initial parameters can barely provide meaningful results due to the presence of barren plateaux, where the mean value of the average energy is -0.1367 after 1,000 iterations across 10 repetitions, as illustrated by the light-blue line in Fig. 3.

V. IDENTIFYING DEGENERATE GROUND STATE SPACE OF QUANTUM MODELS

Deterministic gradient-based optimization methods are predisposed to follow a single path, therefore hampering their ability to efficiently detect multiple optima. A unique advantage of generative models is the ability to produce diverse samples of objects, all of which may minimize objective function. In optimization, this leads to the possibility of finding multiple optimal solutions with a single stage of training. We now show that when appropriately trained, VGON exemplifies such an effective capability for generating multiple (nearly) optimal solutions simultaneously. This capability can be largely ascribed to its integration of

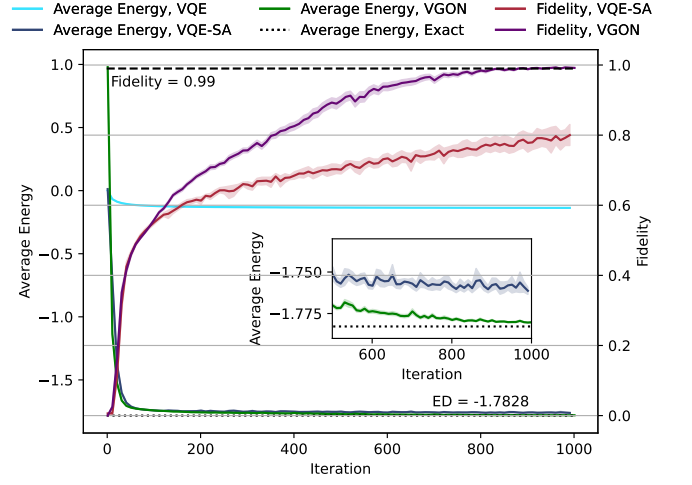


FIG. 3 Mean values and 95% confidence intervals of the energy ground densities and the fidelity to the exact ground state at different iterations. The light-blue line shows the average energy at different iterations for VQE. The dark-blue (red) and the green (purple) lines represent the average energies (fidelity between the produced state and the exact ground state) at different iterations for the VQE-SA method and VGON, respectively. The exact average ground state energy is depicted by the black dots.

randomness and the adoption of batch training. The former facilitates broader exploration within the variational manifold, while the latter, which involves processing subsets of data samples concurrently, supports the collective identification of multiple optimal solutions.

A natural multi-optima problem in quantum many-body physics is the exploration of degenerate ground spaces of quantum many-body Hamiltonians. We apply VGON to two Hamiltonians with known degenerate ground states: the Majumdar-Ghosh (MG) (Majumdar and Ghosh, 1969a,b) model in Eq. (2), and a Heisenberg-like model in Eq. (3) coming from one of the contextuality witnesses presented in Ref. (Yang et al., 2022):

$$H_{MG} = \sum_{i=1}^N \sigma^i \cdot \sigma^{i+1} + \sigma^{i+1} \cdot \sigma^{i+2} + \sigma^i \cdot \sigma^{i+2}, \quad (2)$$

$$H_{232} = \sum_{i=1}^N (2\sigma_x^i \sigma_x^{i+1} + \sigma_x^i \sigma_y^{i+1} - \sigma_y^i \sigma_x^{i+1}), \quad (3)$$

where $\sigma^i = (\sigma_x^i, \sigma_y^i, \sigma_z^i)$ are Pauli operators at site i . We take $N = 10$ for H_{MG} , and $N = 11$ for H_{232} , making their ground state spaces 5- and 2-fold degenerate, respectively. An orthonormal basis for their respective degenerate ground state spaces is computed by the ED method, which outputs five vectors $|v_1\rangle \dots |v_5\rangle$ spanning the ground state space of H_{MG} , and two vectors $|u_1\rangle$ and $|u_2\rangle$ spanning that of H_{232} .

The overall objective of this problem is similar to the previous one: finding the ground states of H_{MG} and H_{232} with variational quantum circuits. We maintain the same circuit

layout as in the previous problem, and use 36 and 60 blocks of unitary gates for each Hamiltonian respectively. Profiting from the use of mini-batches to estimate gradients, a common technique in training neural networks, VGON can effectively evaluate many different circuits simultaneously. Meanwhile, to enhance intra-batch diversity, a penalty term consisting of the mean cosine similarity among all pairs of sets of circuit parameters in the same batch is added to the objective function. This penalty term, together with the mean energy of the states in the batch, ensures a balance between maintaining the diversity of the generated outputs and minimizing the energy. Further details can be found in Appendix D.1.

As a result, unlike VQE-based algorithms aiming to generate multiple energy eigenstates, the objective function of VGON is model-agnostic. In other words, with no prior knowledge of the degeneracy of the ground space, VGON is capable of generating orthogonal or linearly independent states in it. In comparison, to achieve a diversity of outputs with VQE-based algorithms (Higgott *et al.*, 2019; Nakanishi *et al.*, 2019), it is essential to provide diverse inputs for the VQE model. However, attaining this diversity can result in barren plateaux within the optimization landscape. Though employing VQE-SA may address this problem, it could significantly diminish the diversity of inputs, as it tends to constrain inputs to values near zero.

We generate 1,000 output states for each Hamiltonian using a VGON model trained with the above objective function. We find that the vast majority of these states have energy low enough to be treated as ground states. Figure 4 shows the overlap between the generated states and the basis of their ground state space. In Figure 4(a), the generated states for H_{232} fall into two orthogonal classes, which form an orthonormal basis of the ground state space. For H_{MG} , Figure 4(b) shows that most of them are linearly independent and span the same space as $|v_1\rangle \dots |v_5\rangle$.

VI. CONCLUSIONS

We propose a general approach called variational generative optimization network, or VGON for short, for tackling optimization challenges in a variety of quantum problems. This approach combines deep generative models in classical machine learning with sampling procedures and a problem-specific objective function, exhibiting excellent convergence efficiency and solution quality in quantum optimization problems of various sizes. Particularly, it alleviates the barren plateau problem, a pervasive issue in variational quantum algorithms, and surpasses the performance of the VQE-SA method, an approach designed specifically to avoid barren plateaux. Additionally, the capability of VGON to identify degenerate ground states of quantum many-body models underscores its efficacy in addressing problems with multiple optima. Due to its flexible design, we also envisage applying VGON to problems beyond the quantum world,

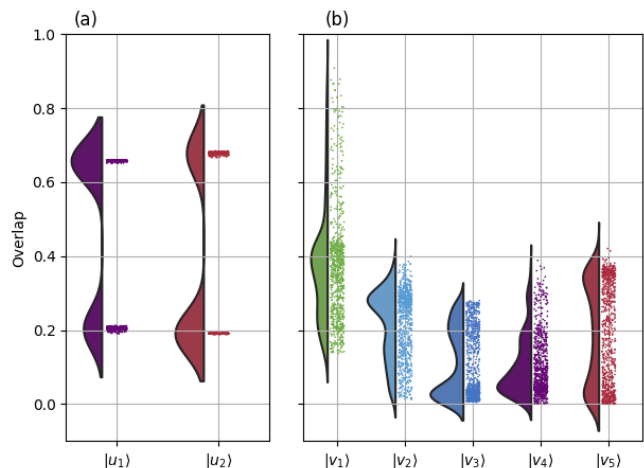


FIG. 4 The overlap between 1,000 states generated by the trained VGON models and the orthonormal bases of the ground space computed by ED: $|u_1\rangle$ and $|u_2\rangle$ for H_{232} shown in (a) and $|v_1\rangle, |v_2\rangle, \dots, |v_5\rangle$ for H_{MG} shown in (b). The shaded curves show the population densities of the generated states having different overlaps with one of the basis states.

particularly those in many areas of science and engineering where high quality multiple optimal solutions are expected.

REFERENCES

- Audet, Charles, and J. E. Dennis (2002), “Analysis of generalized pattern searches,” *SIAM Journal on Optimization* **13** (3), 889–903.
- Bertlmann, Reinhold A, and Philipp Krammer (2008), “Bloch vectors for qudits,” *Journal of Physics A: Mathematical and Theoretical* **41** (23), 235303.
- Bonyadi, Mohammad Reza, and Zbigniew Michalewicz (2017), “Particle swarm optimization for single objective continuous space problems: A review,” *Evolutionary Computation* **25** (1), 1–54.
- Boyd, Stephen, and Lieven Vandenberghe (2004), *Convex Optimization* (Cambridge University Press).
- Carleo, Giuseppe, and Matthias Troyer (2017), “Solving the quantum many-body problem with artificial neural networks,” *Science* **355** (6325), 602–606.
- Carrasquilla, Juan, Giacomo Torlai, Roger G. Melko, and Leandro Aolita (2019), “Reconstructing quantum states with generative models,” *Nature Machine Intelligence* **1** (3), 155–161.
- Cerezo, M, Martin Larocca, Diego García-Martín, N. L. Diaz, Paolo Braccia, Enrico Fontana, Manuel S. Rudolph, Pablo Bermejo, Aroosa Ijaz, Supanut Thanasilp, Eric R. Anschuetz, and Zoë Holmes (2024), “Does provable absence of barren plateaux imply classical simulability? or, why we need to rethink variational quantum computing,” [arXiv:2312.09121 \[quant-ph\]](https://arxiv.org/abs/2312.09121).
- Cerezo, M, Akira Sone, Tyler Volkoff, Lukasz Cincio, and Patrick J. Coles (2021), “Cost function dependent barren plateaux in shallow parametrized quantum circuits,” *Nature Communications* **12** (1), 1791.
- Cirac, J Ignacio, David Pérez-García, Norbert Schuch, and Frank Verstraete (2021), “Matrix product states and projected entan-

- gled pair states: Concepts, symmetries, theorems,” *Rev. Mod. Phys.* **93**, 045003.
- Devroye, Luc (1986), *Non-Uniform Random Variate Generation* (Springer New York, New York, NY).
- Doersch, Carl (2021), “Tutorial on Variational Autoencoders,” [arxiv:1606.05908 \[cs, stat\]](https://arxiv.org/abs/1606.05908).
- Doherty, A C, Pablo A. Parrilo, and Federico M. Spedalieri (2002), “Distinguishing Separable and Entangled States,” *Physical Review Letters* **88** (18), 187904.
- Doherty, Andrew C, Pablo A. Parrilo, and Federico M. Spedalieri (2004), “Complete family of separability criteria,” *Phys. Rev. A* **69**, 022308.
- Farhi, Edward, Jeffrey Goldstone, and Sam Gutmann (2014), “A quantum approximate optimization algorithm,” [arXiv:1411.4028 \[quant-ph\]](https://arxiv.org/abs/1411.4028).
- Gutmann, H M (2001), “A radial basis function method for global optimization,” *Journal of Global Optimization* **19** (3), 201–227.
- Haegeman, Jutho, J. Ignacio Cirac, Tobias J. Osborne, Iztok Pižorn, Henri Verschelde, and Frank Verstraete (2011), “Time-dependent variational principle for quantum lattices,” *Phys. Rev. Lett.* **107**, 070601.
- Hanin, Boris (2018), “Which neural net architectures give rise to exploding and vanishing gradients?” in *Advances in Neural Information Processing Systems*, Vol. 31, edited by S. Bengio, H. Wallach, H. Larochelle, K. Grauman, N. Cesa-Bianchi, and R. Garnett (Curran Associates, Inc.).
- Harrow, Aram W, and Richard A. Low (2009), “Random quantum circuits are approximate 2-designs,” *Communications in Mathematical Physics* **291** (1), 257–302.
- Haug, Tobias, Kishor Bharti, and M.S. Kim (2021), “Capacity and quantum geometry of parametrized quantum circuits,” *PRX Quantum* **2**, 040309.
- Havlíček, Vojtěch, Antonio D. Córcoles, Kristan Temme, Aram W. Harrow, Abhinav Kandala, Jerry M. Chow, and Jay M. Gambetta (2019), “Supervised learning with quantum-enhanced feature spaces,” *Nature* **567** (7747), 209–212.
- Higgott, Oscar, Daochen Wang, and Stephen Brierley (2019), “Variational Quantum Computation of Excited States,” *Quantum* **3**, 156.
- Holmes, Zoë, Kunal Sharma, M. Cerezo, and Patrick J. Coles (2022), “Connecting ansatz expressibility to gradient magnitudes and barren plateaus,” *PRX Quantum* **3**, 010313.
- Hu, Xiao-Min, Yu Guo, Bi-Heng Liu, Yun-Feng Huang, Chuan-Feng Li, and Guang-Can Guo (2018), “Beating the channel capacity limit for superdense coding with entangled ququarts,” *Science Advances* **4** (7), eaat9304.
- Hu, Xiao-Min, Wen-Bo Xing, Yu Guo, Mirjam Weilenmann, Edgar A. Aguilar, Xiaoqin Gao, Bi-Heng Liu, Yun-Feng Huang, Chuan-Feng Li, Guang-Can Guo, Zizhu Wang, and Miguel Navascués (2021), “Optimized Detection of High-Dimensional Entanglement,” *Physical Review Letters* **127** (22), 220501.
- Hyland, Stephanie, and Gunnar Rätsch (2017), “Learning unitary operators with help from $u(n)$,” in *Proceedings of the AAAI Conference on Artificial Intelligence*, Vol. 31, pp. 2050–2058.
- Kandala, Abhinav, Antonio Mezzacapo, Kristan Temme, Maika Takita, Markus Brink, Jerry M. Chow, and Jay M. Gambetta (2017), “Hardware-efficient variational quantum eigensolver for small molecules and quantum magnets,” *Nature* **549** (7671), 242–246.
- Kim, Joonho, Jaedeok Kim, and Dario Rosa (2021), “Universal effectiveness of high-depth circuits in variational eigenproblems,” *Phys. Rev. Res.* **3**, 023203.
- Kingma, Diederik P, and Jimmy Ba (2017), “Adam: A method for stochastic optimization,” [arXiv:1412.6980 \[cs.LG\]](https://arxiv.org/abs/1412.6980).
- Kingma, Diederik P, and Max Welling (2013), “Auto-encoding variational bayes,” [arXiv:1312.6114 \[stat.ML\]](https://arxiv.org/abs/1312.6114).
- Kirkpatrick, S, C. D. Gelatt, and M. P Vecchi (1983), “Optimization by simulated annealing,” *Science* **220** (4598), 671–680.
- Kochenderfer, Mykel J, and Tim A. Wheeler (2019), *Algorithms for Optimization* (The MIT Press, Cambridge, Massachusetts).
- Kolen, John F, and Stefan C. Kremer (2001), “Gradient flow in recurrent nets: The difficulty of learning longterm dependencies,” in *A Field Guide to Dynamical Recurrent Networks* (Wiley-IEEE Press) pp. 237–243.
- Larocca, Martín, Nathan Ju, Diego García-Martín, Patrick J. Coles, and Marco Cerezo (2023), “Theory of overparametrization in quantum neural networks,” *Nature Computational Science* **3** (6), 542–551.
- Li, Shuo-Hui, and Lei Wang (2018), “Neural Network Renormalization Group,” *Physical Review Letters* **121** (26), 260601.
- Luchnikov, Ilia A, Alexander Ryzhov, Pieter-Jan Stas, Sergey N. Filippov, and Henni Ouerdane (2019), “Variational autoencoder reconstruction of complex many-body physics,” *Entropy* **21** (11), 1091.
- Majumdar, Chanchal K, and Dipan K. Ghosh (1969a), “On Next-Nearest-Neighbor Interaction in Linear Chain. I,” *Journal of Mathematical Physics* **10** (8), 1388–1398.
- Majumdar, Chanchal K, and Dipan K. Ghosh (1969b), “On Next-Nearest-Neighbor Interaction in Linear Chain. II,” *Journal of Mathematical Physics* **10** (8), 1399–1402.
- McArdle, Sam, Suguru Endo, Alán Aspuru-Guzik, Simon C. Benjamin, and Xiao Yuan (2020), “Quantum computational chemistry,” *Rev. Mod. Phys.* **92**, 015003.
- McClean, Jarrod R, Sergio Boixo, Vadim N. Smelyanskiy, Ryan Babbush, and Hartmut Neven (2018), “Barren plateaus in quantum neural network training landscapes,” *Nature Communications* **9** (1), 4812.
- Melko, Roger G, Giuseppe Carleo, Juan Carrasquilla, and J. Ignacio Cirac (2019), “Restricted Boltzmann machines in quantum physics,” *Nature Physics* **15** (9), 887–892.
- Milsted, Ashley, Jutho Haegeman, Tobias J. Osborne, and Frank Verstraete (2013), “Variational matrix product ansatz for nonuniform dynamics in the thermodynamic limit,” *Phys. Rev. B* **88**, 155116.
- Mitchell, Melanie (1998), *An Introduction to Genetic Algorithms* (MIT Press, Cambridge, MA, USA).
- Murphy, Kevin P (2022), *Probabilistic Machine Learning: An introduction* (MIT Press).
- Nakanishi, Ken M, Kosuke Mitarai, and Keisuke Fujii (2019), “Subspace-search variational quantum eigensolver for excited states,” *Phys. Rev. Res.* **1**, 033062.
- Navascués, Miguel, Stefano Pironio, and Antonio Acín (2007), “Bounding the set of quantum correlations,” *Phys. Rev. Lett.* **98**, 010401.
- Ortiz Marrero, Carlos, Mária Kieferová, and Nathan Wiebe (2021), “Entanglement-induced barren plateaus,” *PRX Quantum* **2**, 040316.
- Peruzzo, Alberto, Jarrod McClean, Peter Shadbolt, Man-Hong Yung, Xiao-Qi Zhou, Peter J. Love, Alán Aspuru-Guzik, and Jeremy L. O’Brien (2014), “A variational eigenvalue solver on a photonic quantum processor,” *Nature Communications* **5** (1), 4213.
- Radford, Alec, Karthik Narasimhan, Tim Salimans, and Ilya Sutskever (2017), “Improving Language Understanding by Generative Pre-Training,” OpenAI Preprint.
- Ran, Shi-Ju (2020), “Encoding of Matrix Product States into Quantum Circuits of One- and Two-Qubit Gates,” *Physical Review A* **101** (3), 032310.

- Rocchetto, Andrea, Edward Grant, Sergii Strelchuk, Giuseppe Carleo, and Simone Severini (2018), “Learning hard quantum distributions with variational autoencoders,” *npj Quantum Information* **4** (1), 28.
- Romero, Jonathan, Ryan Babbush, Jarrod R McClean, Cornelius Hempel, Peter J Love, and Alán Aspuru-Guzik (2018), “Strategies for quantum computing molecular energies using the unitary coupled cluster ansatz,” *Quantum Science and Technology* **4** (1), 014008.
- Romero, Jonathan, Jonathan P Olson, and Alan Aspuru-Guzik (2017), “Quantum autoencoders for efficient compression of quantum data,” *Quantum Science and Technology* **2** (4), 045001.
- Sá, Nahum, and Itzhak Roditi (2021), “ β -variational autoencoder as an entanglement classifier,” *Physics Letters A* **417**, 127697.
- Sack, Stefan H, Raimel A. Medina, Alexios A. Michailidis, Richard Kueng, and Maksym Serbyn (2022), “Avoiding barren plateaus using classical shadows,” *PRX Quantum* **3**, 020365.
- Schuld, Maria, Alex Bocharov, Krysta M. Svore, and Nathan Wiebe (2020), “Circuit-centric quantum classifiers,” *Phys. Rev. A* **101**, 032308.
- Stornati, Paolo (2022), *Variational Quantum Simulations of Lattice Gauge Theories*, Ph.D. thesis (Humboldt-Universität zu Berlin).
- Taube, Andrew G, and Rodney J. Bartlett (2006), “New perspectives on unitary coupled-cluster theory,” *International Journal of Quantum Chemistry* **106** (15), 3393–3401.
- Tavakoli, Armin, Alejandro Pozas-Kerstjens, Peter Brown, and Mateus Araújo (2023), “Semidefinite programming relaxations for quantum correlations,” [arxiv:2307.02551 \[quant-ph\]](https://arxiv.org/abs/2307.02551).
- Ugray, Zsolt, Leon Lasdon, John Plummer, Fred Glover, James Kelly, and Rafael Martí (2007), “Scatter search and local nlp solvers: A multistart framework for global optimization,” *INFORMS Journal on Computing* **19** (3), 328–340.
- van Esbroeck, N M, D T Lennon, H Moon, V Nguyen, F Vigneau, L C Camenzind, L Yu, D M Zumbühl, G A D Briggs, D Sejdinovic, and N Ares (2020), “Quantum device fine-tuning using unsupervised embedding learning,” *New Journal of Physics* **22** (9), 095003.
- Vanderstraeten, Laurens, Jutho Haegeman, and Frank Verstraete (2019), “Tangent-space methods for uniform matrix product states,” *SciPost Physics Lecture Notes* , 7.
- Vaswani, Ashish, Noam Shazeer, Niki Parmar, Jakob Uszkoreit, Llion Jones, Aidan N. Gomez, Łukasz Kaiser, and Illia Polosukhin (2017), “Attention is all you need,” in *Proceedings of the 31st International Conference on Neural Information Processing Systems, NIPS’17* (Curran Associates Inc., Red Hook, NY, USA) pp. 6000–6010.
- Weilenmann, M, E. A. Aguilar, and M. Navascués (2021), “Analysis and optimization of quantum adaptive measurement protocols with the framework of preparation games,” *Nature Communications* **12** (1), 4553.
- White, Steven R (1992), “Density matrix formulation for quantum renormalization groups,” *Phys. Rev. Lett.* **69**, 2863–2866.
- Yang, Kaiyan, Xiao Zeng, Yujing Luo, Guowu Yang, Lan Shu, Miguel Navascués, and Zizhu Wang (2022), “Contextuality in infinite one-dimensional translation-invariant local hamiltonians,” *npj Quantum Information* **8** (1), 89.

Appendix A: Reaching the quantum limit of a many-body contextuality witness

Contextuality, a variant of quantum nonlocality when space-like separation can not be guaranteed, can be certified by the violation of a kind of inequalities called contextuality witnesses. For example, a typical contextuality witness is given by (Yang *et al.*, 2022)

$$\begin{aligned} & -4\langle O_b^1 \rangle + 2\langle O_a^1 O_a^2 \rangle + 2\langle O_a^1 O_b^2 \rangle - 2\langle O_b^1 O_a^2 \rangle + 2\langle O_b^1 O_b^2 \rangle \\ & + \langle O_a^1 O_b^3 \rangle - \langle O_b^1 O_a^3 \rangle \geq -4, \end{aligned} \quad (\text{A1})$$

where $\{\langle O_x^1 \rangle : x \in \{a, b\}\}$, $\{\langle O_x^1 O_y^2 \rangle : x, y \in \{a, b\}\}$ and $\{\langle O_x^1 O_y^3 \rangle : x, y \in \{a, b\}\}$ are the expectations of single-site correlator, nearest-neighbor and next-to-nearest neighbor two-point correlators, respectively.

Ref. (Yang *et al.*, 2022) shows that for a given contextuality witness, the strongest violation that a quantum many-body system exhibits can be characterized as below. First, we transform the contextuality witness into a 1D infinite translation-invariant (TI) Hamiltonian with the fixed couplings being the same as the coefficients in the contextuality witness. Second, we choose the optimal local observables for the Hamiltonian such that the ground state energy density (GSED) is the lowest.

For example, we can parameterize the local observables $O_x : x \in \{a, b\}$ as

$$O_x(\theta_x) = (e^{\sum_{j=1}^m \theta_{xj} S_j}) \Lambda_x (e^{\sum_{j=1}^m \theta_{xj} S_j})^T, \quad (\text{A2})$$

where Λ_x is a diagonal matrix with entries being ± 1 , $\{S_j\}$ are the basis of the space of skew-symmetric matrices with the dimension of $m = (d^2 - d)/2$, d is the local dimension, and $\theta_x \equiv (\theta_{x1}, \theta_{x2}, \dots, \theta_{xm})$ are real scalars. All the parameters combined are denoted as $\theta \equiv (\theta_a, \theta_b)$. Then the Hamiltonian corresponding to contextuality witness (A1) can be expressed as

$$\begin{aligned} H(\theta) = & \sum_{i=1}^{\infty} -4O_b^i(\theta_b) + 2O_a^i(\theta_a)O_a^{i+1}(\theta_a) + 2O_a^i(\theta_a)O_b^{i+1}(\theta_b) \\ & - 2O_b^i(\theta_b)O_a^{i+1}(\theta_a) + 2O_b^i(\theta_b)O_b^{i+1}(\theta_b) \\ & + O_a^i(\theta_a)O_b^{i+2}(\theta_b) - O_b^i(\theta_b)O_a^{i+2}(\theta_a), \end{aligned} \quad (\text{A3})$$

where $O_a^i(\theta_a)$ and $O_b^i(\theta_b)$ are two dichotomic observables on site i . We denote its GSED by $e(H(\theta))$, which can be calculated by the time-dependent variational principle (TDVP) algorithms (Haegeman *et al.*, 2011; Milsted *et al.*, 2013).

As a result, finding the strongest violation to the contextuality witness in Eq. (A1) is now equivalent to solving the following minimization problem:

- **Objective function:** $h(\theta) = e(H(\theta))$
- **Parameter space:** $\{\theta \in \mathbb{R}^{d^2-d}\}$

In fact, by a modified version of the Navascués-Pironio-Acín (NPA) hierarchy (Yang *et al.*, 2022), a lower bound

for the lowest GSED of $H(\theta)$ has been obtained to be -4.4142134689 . However, whether there is any infinite TI quantum many-body Hamiltonian can achieve this bound is still unknown. Using stochastic gradient descent (SGD), Ref. (Yang *et al.*, 2022) reports an infinite TI model that the corresponding GSED is -4.4142131947 , which has a physical dimension $d = 5$ and a bond dimension $D = 5$.

Combining these two results together, we can pin down the lowest GSED of $H(\theta)$ to the seventh significant digit.

We apply VGON to the above optimization problem. The model we choose contains a 2-layer encoder network with sizes $[8, 4]$, a latent space with dimension 2, and a 3-layer decoder network with sizes $[4, 8, 16]$. In addition, we set the batch size as 2 and the learning rate as 0.005. It turns out that among all the outputs generated by VGON, 100% can achieve a GSED of -4.4142134 , improving the precision to eight significant digits.

Appendix B: Finding the optimal state for entanglement detection

Suppose Alice and Bob are separated physically and want to determine whether a shared quantum state is entangled or not. For this, they play the prepare-and-measure entanglement detection game, where their goal is to design powerful measurement protocols such that the probability that they make mistakes is minimized.

In a typical hypothesis test, all errors can be classified into two categories: type-I error (false-positive statistical error, i.e., concluding "Yes" when the state is not entangled) and type-II error (false-negative statistical error, i.e., concluding "No" when the state is entangled).

On a given quantum state ρ , in order to compare the power of local operations and one-way classical communication (1-LOCC) protocols and that of local operations (LO) ones on this problem, we can first fix the type-I error probability to be p_1 , and then compare the minimal type-II error probability p_2^* that these two kind of protocols can achieve. Furthermore, it has been known that p_2^* can be calculated by the following semidefinite programming (SDP) optimization problems:

$$\begin{aligned} & \min p_2 \\ & \text{subject to } \text{tr}(M_N \rho) = p_2, p_1 \mathbb{I} - M_Y \in \mathcal{S}^*, \\ & M_Y = M_Y(P), M_N = M_N(P), \\ & P \in \mathcal{P}^{\{LO, 1-LOCC\}}. \end{aligned} \quad (\text{B1})$$

Here $M_{Y(N)}$ is the positive operator-valued measure (POVM) operator with the outcome "Yes" (or "No") and can be expressed as a linear combination of variable P and the measurement operators $\{A_x^a\}$ ($\{B_y^b\}$) implemented in Alice's (Bob's) side, i.e.,

$$M_{Y(N)}(P) = \sum_{x,y,a,b} P(x, y, \gamma = Y(N)|a, b) A_x^a \otimes B_y^b,$$

where x (y) denotes the label of the measurement settings, and a (b) denotes the corresponding outcomes.

In addition, for different protocols the set of feasible optimization variables $P \in \mathcal{P}^{\{LO,1-LOCC\}}$ is restricted by different physical constraints. In LO protocols, the variable P is required to satisfy

$$\sum_{\gamma} P(x, y, \gamma|a, b) = P(x, y), \quad \sum_{x,y} P(x, y) = 1,$$

while for 1-LOCC protocols, we suppose that Alice makes the measurement first and then sends her measurement setting x and outcome a to Bob, making P satisfy

$$\begin{aligned} \sum_{\gamma} P(x, y, \gamma|a, b) &= P(x, y|a), \quad \sum_y P(x, y|a) = P(x), \\ \sum_x P(x) &= 1. \end{aligned}$$

Meanwhile, recall that the separable set is characterized by a hierarchical manner (Doherty *et al.*, 2002, 2004). Taking the first level of hierarchical characterization into consideration, the constraint $p_1 \mathbb{I} - M_Y \in \mathcal{S}^*$ is dually equivalent to that the semidefinite positive matrices M_0 and M_1 satisfy

$$p_1 \mathbb{I} - M_Y = M_0 + M_1^{T_B},$$

where T_B denotes the partial transpose with respect to Bob's subsystem.

As a result, when quantifying the advantage of 1-LOCC protocols over LO ones in detecting the entanglement of ρ , we can focus on the following two SDP optimization problems and compute the gap between their solutions:

$$\begin{aligned} &\min_{P, M_0, M_1} P_2 \\ \text{subject to} &\quad \text{tr}(M_N \rho) = p_2 \\ &\quad p_1 \mathbb{I} - M_Y = M_0 + M_1^{T_B}, \quad M_0, M_1 \succcurlyeq 0 \\ &\quad M_Y = \sum_{x,y,a,b} P(x, y, \gamma = Y|a, b) A_x^a \otimes B_y^b. \quad (\text{B2}) \\ &\quad M_N = \sum_{x,y,a,b} P(x, y, \gamma = N|a, b) A_x^a \otimes B_y^b \\ &\quad P(x, y, \gamma|a, b) \geq 0, \quad P \in \mathcal{P}^{\{LO,1-LOCC\}} \end{aligned}$$

Additionally, to make a fair comparison, in both 1-LOCC and LO protocols Alice and Bob choose the same set of quantum measurement settings as below:

$$\begin{aligned} A_1^1 &= |0\rangle, \quad A_1^2 = |1\rangle, \quad A_1^3 = |2\rangle, \\ A_2^1 &= \frac{1}{\sqrt{3}}(|0\rangle + e^{-i\frac{2\pi}{3}}|1\rangle + e^{-i\frac{2\pi}{3}}|2\rangle), \\ A_2^2 &= \frac{1}{\sqrt{3}}(|0\rangle + e^{-i\frac{2\pi}{3}}|1\rangle + e^{-i\frac{2\pi}{3}}|2\rangle), \\ A_2^3 &= \frac{1}{\sqrt{3}}(|0\rangle + |1\rangle + |2\rangle), \\ A_3^1 &= \frac{1}{\sqrt{2}}(|1\rangle - |2\rangle), \quad A_3^2 = |0\rangle, \quad A_3^3 = \frac{1}{\sqrt{2}}(|1\rangle + |2\rangle). \end{aligned}$$

In this work, we would also like to observe the advantage of 1-LOCC protocols over LO ones in quantum experiments. However, for a typical quantum state ρ the above gap is very small, which makes the experimental observations very challenging, considering the imperfections of instruments and experimental noises. Therefore, we need to search for a quantum state that maximizes the above gap. Meanwhile, due to the limitations in experimental state preparations, we have to make the optimization among experiment-friendly states only.

We employ both SGD and VGON to search for the optimal experiment-friendly pure state to exhibit the advantage of 1-LOCC protocols. Our results show that the VGON model is capable of generating the best pure states in approximately two hours, whereas it takes SGD over two months to achieve the same results. This sharp comparison highlights the significant advantage of VGON over the SGD method in tackling this problem.

Rigorously speaking, however, we cannot ensure that the optimal advantage is achieved by pure states, hence we also run VGON to search the maximal gap in the submanifold of mixed states space. Interestingly, numerical calculations show that this does not increase the observed gap further, implying that the largest gap is indeed achieved by pure quantum states.

1. The pure state case

In a typical quantum laboratory, usually only a fraction of all quantum states can be prepared conveniently. Taking the photonic platform as an example, photons generated by the source interfere with each other and produce a quantum state expressed as $\sum_i c_i |ii\rangle$, where c_i are complex numbers satisfying $\sum_i |c_i|^2 = 1$. Then it can be transformed to $|\psi\rangle = \sum_i c_i |ii\rangle$ through spontaneous parametric down-conversion (SDPC). Specifically, when $|\psi\rangle$ is a qutrit-qutrit quantum system, it can be parameterized as (Hu *et al.*, 2018, 2021)

$$|\psi\rangle = \sin \frac{\theta}{2} \cos \frac{\phi}{4} e^{im} |00\rangle + \sin \frac{\theta}{2} \sin \frac{\phi}{4} e^{in} |11\rangle + \cos \frac{\theta}{2} |22\rangle,$$

where $\phi, m, n \in [0, 2\pi)$, and $\theta \in [0, \pi]$. Then two local unitaries denoted by U_A, U_B can be applied on the two subsystems, resulting in the quantum state

$$\rho_{\text{exp}} = (U_A \otimes U_B) |\psi\rangle \langle \psi| (U_A^\dagger \otimes U_B^\dagger).$$

Here U_A (U_B) can be parameterized by a set of $3^2 = 9$ linearly-independent skew-Hermitian matrices $\{T_j\}$ (Hyland and Ratsch, 2017), i.e.,

$$U_A (U_B) = \exp \left(\sum_{j=1}^9 \lambda_j T_j \right),$$

where λ_j 's are 9 real numbers, denoted as λ_A (λ_B).

Then the problem is formulated as the following maximization problem:

- **Objective function:** $h(\rho_{\text{exp}}, p_1) = p_2^{LO*}(\rho_{\text{exp}}, p_1) - p_2^{1-LOCC*}(\rho_{\text{exp}}, p_1)$
- **Parameter space:** $\{e_1, m, n, \phi, \theta \in \mathbb{R}, \lambda_A, \lambda_B \in \mathbb{R}^9\}$.

Here we set $p_1 = (\tanh(e_1) + 1)/2$, and p_2^{LO*} and $p_2^{1-LOCC*}$ are computed by solving the two SDPs in Eq. (B2) respectively.

To fully test the performance of SGD on this problem, we run this algorithm for 79,663 different initial states, which are sampled from the parameter space according to the distribution $\mathcal{N}(\mathbf{0}, \mathbf{I})$. The results are listed in Fig. 5(a), where the green and the blue dots present the gaps for the initial states and the optimized states, respectively. It turns out that GD gets stuck in local minima easily, and only 1.52% of the initial states achieve a gap larger than 0.08. The largest gap observed is 0.0837. Lastly, we would like to stress that the above calculations take more than two months on a desktop-grade computer.

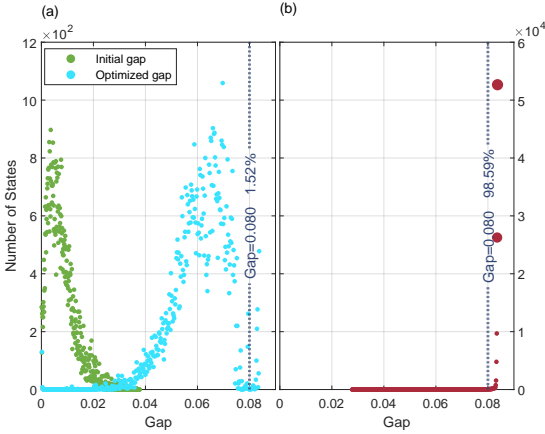


FIG. 5 Distributions of gaps achieved by SGD and VGON. (a) Distributions of gaps obtained by SGD in two months. The green and blue dots present the gaps achieved by the 79,663 initial states of SGD and those by the corresponding optimized states, respectively. 1.52% of them achieve a gap larger than 0.08, which is represented by the dark-blue dotted line. The obtained maximal gap is roughly 0.0837. (b) Distributions of the gaps optimized by VGON in two hours. Remarkably, 98.59% of them exceed 0.08, and 52.657% of them even fall within the range $[0.0836, 0.0837]$.

Subsequently, the same problem is addressed by VGON. The architecture of the VGON model consists of a 3-layer encoder network with sizes $[512, 256, 128]$, a 3-layer decoder network with sizes $[128, 256, 512]$, and a 2-dimensional latent space connecting the encoder and decoder components. The training is conducted with a batch size of 6, and an exponential decaying learning rate lr_i at iteration i , where $lr_i = 0.99 \times lr_{i-1}$, and $lr_1 = 0.001$. Once trained, the VGON model generates 100,000 quantum states as the output, and the gaps achieved by these quantum states are listed in Fig. 5(b), where we can see that the performance of VGON overwhelmingly surpasses that of the GD method.

Specifically, 98.59% of the quantum states that VGON generates exhibit a gap larger than 0.08, and 52.657% of them even fall within the range $[0.0836, 0.0837]$, which is also the maximal gap found by SGD.

2. The mixed state case

A subset of mixed quantum state $\rho \in \mathcal{H}^3 \otimes \mathcal{H}^3$ can be parameterized by

$$\rho = U \Sigma U^\dagger, \quad (\text{B3})$$

where Σ is a 9×9 diagonal matrix whose diagonal entries are nonnegative and sum to 1, and U is a unitary matrix that can be parameterized by a set of $9^2 - 1$ generalized Gell-Mann matrices $\{T_j\}$ (Bertlmann and Krammer, 2008), i.e.,

$$U = \exp \left(i \sum_{j=1}^{9^2-1} \lambda_j T_j \right),$$

where λ_j 's are $9^2 - 1$ real numbers, denoted as $\lambda \in \mathbb{R}^{9^2-1}$.

We search for the mixed quantum state that achieves the largest gap with different methods including VGON. In order to facilitate the parameter update during the optimization process, we again set p_1 as $(\tanh(e_1) + 1)/2$, and write Σ as $\text{diag}(\sigma_1^2, \dots, \sigma_9^2)$. If we let $\sigma = (\sigma_1, \dots, \sigma_9)$, then it holds that $\|\sigma\|_2 = 1$. In this way, the problem is formed as the following maximization problem

- **Objective function:** $h(\rho, p_1) = p_2^{LO*}(\rho, p_1) - p_2^{1-LOCC*}(\rho, p_1)$
- **Parameter space:** $\{e_1 \in \mathbb{R}, \lambda \in \mathbb{R}^{9^2-1}, \sigma \in \mathbb{R}^9 : \|\sigma\|_2 = 1\}$

For such a task, the chosen VGON model comprises a 4-layer encoder network and a 3-layer decoder network with sizes $[1024, 512, 256, 128]$ and $[128, 256, 512]$ respectively. We maintain the same latent space dimension and the same learning rate as those used in the training for pure states. In addition, we train the VGON model with a batch size of 3. Our results are depicted in Fig. 6(a), which indicates that the VGON model is exceptionally adept at performing this task. Notably, 99.98% of the parameter sets generated by the VGON model manifest a gap of 0.07, and 99.32% of them even surpass a gap of 0.08. Particularly, as shown in Fig. 6(b), when starting from a variational submanifold of the space of all mixed states, VGON always identified an almost pure state maximizing the gap, where the minimum achieved purity is 0.9993, and 96.49% of the states have a purity greater than 0.9999. This shows the excellent capability of VGON in identifying qualified quantum states from the complex quantum state landscape without being stuck in local minima.

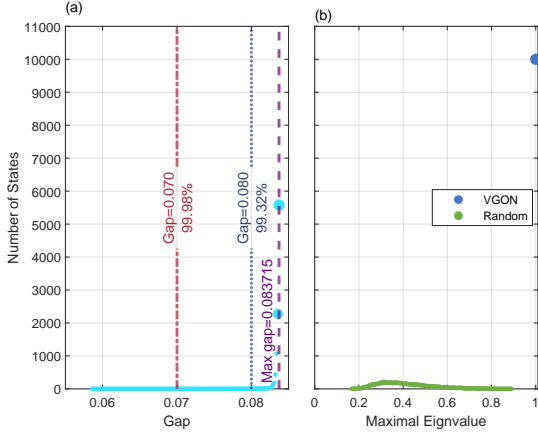


FIG. 6 Numerical results for exhibiting the advantage of 1-LOCC over LO. (a) Distribution of the advantage brought by the VGON. (b) Distributions of the maximal eigenvalues for random training states and those generated by the VGON.

For comparison purposes, we also apply seven other global optimization algorithms to this problem. For gradient-based algorithms, we choose GlobalSearch and Multistart (Ugray *et al.*, 2007), which both run repeatedly in parallel and attempt to find multiple local solutions with the help of certain strategies for choosing starting points. For gradient-free algorithms, we focus on Genetic Algorithm (GA) (Mitchell, 1998), Particle Swarm Optimization (PSO) (Bonyadi and Michalewicz, 2017), Simulated Annealing (SA) (Kirkpatrick *et al.*, 1983), Pattern Search (PS) (Audet and Dennis, 2002) and Surrogate optimization (SO) (Gutmann, 2001). Since these algorithms are gradient-free, the updates of parameters are relatively easy to compute, while the optimization directions may not be accurate.

Additionally, Multilayer Perceptron (MLP) is also employed, which is a simple artificial neural network consisting of multiple fully connected layers.

Using the default settings of the programs implemented by MATLAB, all the global optimization algorithms are executed on a computer with an Intel i9-12900KS Core and a RAM of 128 GB for 24 hours. Meanwhile, an MLP model consisting of a 7-layer network with each layer containing 90 neurons is also trained 10 times with the other configuration remaining the same as that of VGON. The numerical results are shown in Table. II, where we can clearly see that the performance of VGON exceeds that of all the other methods.

Appendix C: Alleviating the effect of barren plateaux in variational quantum algorithms

The aim of the variational quantum eigensolver (VQE) is to approximate the ground state $|\psi_G\rangle$ of a target Hamiltonian H with a variational wave function

TABLE II Comparisons of VGONs with seven global optimization algorithms and MLP

Algorithm	Maximal Optimized Gap	Run time
GlobalSearch	1.2e-07	24 hours
Multistart	0.0726	24 hours
GA	0.0779	24 hours
PSO	0.0348	24 hours
SA	0.0067	24 hours
PS	0.0717	24 hours
SO	0.0412	24 hours
MLP	0.0384	3000 iterations
VGON	0.0837	3000 iterations

$$|\psi(\theta)\rangle = U(\theta)|00\cdots 0\rangle,$$

where variational parameters $\theta \in \mathbb{R}^M$, and M is determined by the practical ansatz of the parameterized quantum circuit (PQC). To ensure a close approximation to the ground state, θ is iteratively updated through a classical computer by a gradient descent algorithm aiming at minimizing the energy, which forces $|\psi(\theta)\rangle$ to be close to the ground state $|\psi_G\rangle$. More concretely, the optimization problem is formed as the following minimization problem:

- **Objective function:** $h(\theta) = \langle \psi(\theta) | H | \psi(\theta) \rangle$
- **Parameter space:** $\{\theta \in \mathbb{R}^M\}$

However, gradient-based optimization methods often encounter a notable challenge called barren plateaux (BPs), which are characterized by exponentially vanishing gradients. This issue typically emerges from random initializations of parameterized unitaries that admit the statistics of a unitary 2-design (Harrow and Low, 2009).

In this section, we first apply PQCs on large-scale quantum problems to replicate the BP phenomenon, where the magnitude of parameters, M , reaches up to 10^4 . Then we show that the VGON model can address this challenge very well, which not only showcases its capacity to handle large-scale optimization problems, but also highlights its critical advantage in overcoming the issue of gradient vanishing.

1. The $Z_1 Z_2$ model

As a toy example, we first set the target Hamiltonian to be

$$H = Z_1 Z_2,$$

i.e., a Pauli ZZ operator acting on the first and second qubits, and the corresponding ground energy is -1. This Hamiltonian was studied in Ref. (McClean *et al.*, 2018) to exhibit the existence of BPs.

To approximate the ground states of Z_1Z_2 , a hardware-efficient ansatz (Kandala *et al.*, 2017)

$$U(\theta) = \prod_{l=1}^L U_{ENT} \left(\prod_{i=1}^N R_l^i(\theta_l^i) \right),$$

is adopted. Here $\theta_l^i \in [0, 2\pi)$ are variational angles, and all the $L \times N$ such angles combined is denoted as θ . The rotations $R_l^i(\theta_l^i) = \exp(-\frac{i}{2}\theta_l^i G_l^i)$ have random directions given by $G_l^i \in \{\sigma_x, \sigma_y, \sigma_z\}$. U_{ENT} is an entangling unitary operation consisting of two-qubit nearest-neighbor controlled-Z (CZ) gates with periodic boundary conditions. L and N correspond to the numbers of the layers and qubits of $U(\theta)$ respectively. The structure of $U(\theta)$ for the Z_1Z_2 model is schematically shown in Fig. 7.

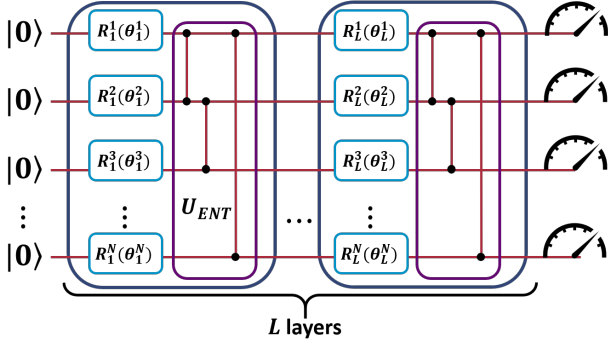


FIG. 7 Structure of the parameterized quantum circuit for the Z_1Z_2 model. Each dark-blue wireframe represents a layer of the circuit consisting of single-qubit rotations represented by light-blue boxes and an entangling unitary operation U_{ENT} represented as a purple box, where entangling CZ gates are shown by lines. The measurements at the end are used to estimate the energy of the trial state.

Let the numbers of qubits and layers be 20 and 400 respectively. To approximate the ground states of the Z_1Z_2 model by VQE, the variable $\theta \in \mathbb{R}^{8,000}$ is uniformly initialized from the parameter space, i.e., $\theta_l^i \in [0, 2\pi)$, and then updated iteratively by the Adam optimizer (Kingma and Ba, 2017) to minimize $h(\theta)$. After 300 iterations, the obtained energy is -0.0068, which is actually far from the ground energy -1. Particularly, the variance of $\{\partial_{\theta_l^i} h(\theta)\}$ decreases from 4.4999×10^{-7} right after the initialization to 1.3351×10^{-9} at the last iteration, which indicates that VQE suffers from BPs heavily, hence can hardly achieve the ground energy. The dark-blue boxes in Fig. 8 and the dark-blue line in Fig. 9 plot these numerical results, which also match the results reported in Ref. (McClellan *et al.*, 2018).

Meanwhile, several promising strategies for avoiding BPs have been proposed and investigated, and small-angle initialization, denoted as VQE-SA, is a widely used technique (Haug *et al.*, 2021; Holmes *et al.*, 2022; Sack *et al.*, 2022). The VQE-SA method tries to initialize θ near the zero vector, thus differing the statistics of $U(\theta)$ from a 2-design to avoid BPs.

We now apply VGON to solve the same problem. Since VGON is designed to map a bunch of different initial values of the variable θ to the optimal ones, it may break improper initializations of random quantum circuits that lead to BPs. Besides, VGON contains a sampling procedure in the latent space to bring randomness, which may also help to maintain larger gradients. Interestingly, we will show that this is indeed the case, and VGON not only can solve the Z_1Z_2 model very well, but also enjoys a remarkable advantage over the VQE-SA method in alleviating BPs.

To employ the VQE-SA method on this problem, the variable θ is uniformly sampled from $\{\theta_l^i \in [0, 0.01]\}$ as the starting point, and then updated iteratively to minimize $h(\theta)$. As for VGON, 1,200 θ 's are uniformly initialized from $\{\theta_l^i \in [0, 2\pi)\}$ as inputs of the VGON model, whose structure contains a 4-layer encoder network with layer shape [256, 128, 64, 32], a latent space with dimension 3, and a 4-layer decoder network with layer shape [32, 64, 128, 256]. Set batch size to be 4, and the coefficient of the KL divergence to be 1/8. With all the other configurations kept the same as the VQE method introduced above, we run both the VQE-SA method and VGON for 300 iterations. Note that the update for one batch in VGON counts for one iteration.

To fairly compare the gradient distributions of the two optimization algorithms, we focus on $\{\partial_{\theta_l^i} h(\theta)\}$ for the VQE-SA method, and $\{\partial_{b_l^i} C(\phi, \omega)\}$ for VGON, where b_l^i is the bias in the last layer of the decoder that contributes to the parameter θ_l^i . To explain why this is the case, notice that

$$\theta_l^i = W^{(l,i)} \mathbf{x} + b_l^i,$$

where $W^{(l,i)}$ represents a row of the weight matrix of the decoder's last layer and \mathbf{x} is the output of the previous layer. Therefore, $\partial_{b_l^i} C(\phi, \omega)$ is influenced by the PQC $U(\theta)$ only, making the comparison with $\partial_{\theta_l^i} h(\theta)$ quite fair.

It turns out that right after the initialization, the variances of these two sets of gradients are 1.0695×10^{-2} and 1.2742×10^{-2} , respectively, which are both five orders of magnitude larger than those in the original VQE method. When the optimizations are terminated, these variances eventually decrease to 7.8099×10^{-14} and 6.0972×10^{-6} , respectively, with only VGON exhibiting a much larger variance magnitude than VQE. Fig. 8 illustrates the distribution of $\{|\partial_{\theta_l^i} h(\theta)|\}$ for the VQE-SA method with red boxplots, and that of $\{|\partial_{b_l^i} C(\phi, \omega)|\}$ for VGON with purple boxplots. As we can see, the absolute values of the gradients for the VQE-SA method and VGON are distributed more widely than those in VQE. Furthermore, a considerable part of these absolute values of gradients, especially at the initial stages, is several orders of magnitude larger compared to those in VQE, which is crucial for effectively decreasing the energies.

In addition, Fig. 9 illustrates the energies at different iterations for the two methods. As depicted by the red dashed line, the VQE-SA method converges to -1 fast, which is exactly the ground energy. In VGON, the average (minimal)

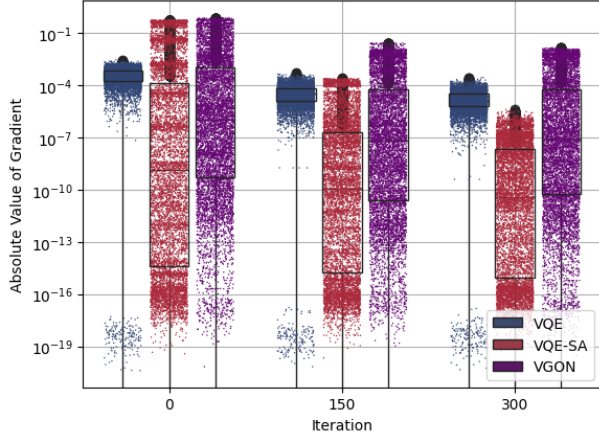


FIG. 8 The absolute values of the gradients for the Z_1Z_2 model. The boxplots illustrate the distribution of $\{|\partial_{\theta_i} h(\theta)|\}$ for VQE (dark-blue) and the VQE-SA method (red), and the distribution of $\{|\partial_{\theta_i} C(\phi, \omega)|\}$ for the VGON (purple) at different iterations. Each boxplot displays the distribution based on a five-number summary: the minimum, the first quartile, the sampled median, the third quartile and the maximum. All other observed data points outside the minimum and maximum are plotted as outliers with black diamonds.

energy is represented by the green (purple) dashed line, which also decreases rapidly, and eventually achieves a minimum value of -0.9998 (-0.9999). Compared with the VQE-SA method, at the beginning the fluctuations in VGON are smaller, which means VGON converges to the ground energy faster in this stage. However, since VGON tries to map the uniformly random parameters to those centered around the optimal parameters, there remain weak fluctuations in the later stage, but it still manages to find the ground energy very well.

2. The Heisenberg XXZ model

On the Z_1Z_2 model, VGON exhibits its advantage over VQE, but the separation between it and VQE-SA in terms of convergence speed is less obvious. To further investigate the advantage, we now move on to the Heisenberg XXZ model, and compare the performance of different methods from the perspective of the fidelity between the optimized state and the exact ground state.

The Hamiltonian of the Heisenberg XXZ model with periodic boundary conditions is given by

$$H_{XXZ} = - \sum_{i=1}^N (\sigma_x^i \sigma_x^{i+1} + \sigma_y^i \sigma_y^{i+1} - \sigma_z^i \sigma_z^{i+1}),$$

where $\sigma_{x,y,z}^i$ denote the Pauli operators at site i . For the number of qubits $N = 18$, the exact average ground energy is -1.7828 .

To find out the ground state of H_{XXZ} , a relatively more

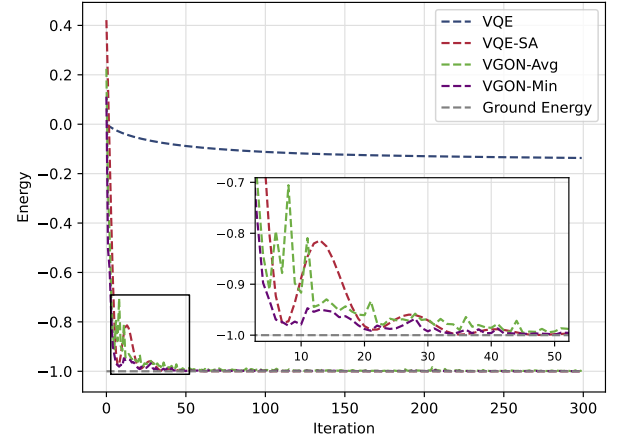


FIG. 9 Energies of the Z_1Z_2 model at different iterations for different methods. The VQE (dark-blue) suffers from BPs and can hardly be optimized. The VQE-SA method (red) and VGON, whose average (green) and minimal (purple) energies in each batch are presented, converge to the ground energy quickly. The exact ground energy (gray) is -1 .

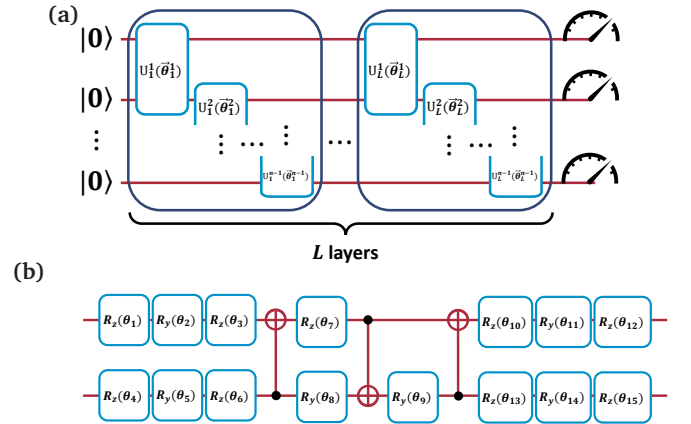


FIG. 10 Structure of the parameterized quantum circuit for the Heisenberg XXZ model. (a) Each dark-blue box represents a layer of the circuit consisting of $n - 1$ universal 2-qubit gate blocks. (b) Each universal 2-qubit gate block is decomposed into 15 rotation gates and 3 CNOT gates.

complex ansatz (Ran, 2020)

$$U'(\theta) = \prod_{l=1}^L \prod_{i=1}^{N-1} U_l^i(\theta_l^i) \quad (C1)$$

depicted in Fig. 10 (a) is applied. Here L and N are the numbers of the layers and qubits involved in $U'(\theta)$ respectively, and each $U_l^i(\theta_l^i)$ is a universal 2-qubit gate at the l -th layer acting on qubits i and $i + 1$, which is determined by θ_l^i containing 15 rotation angles, as illustrated in Fig. 10 (b).

Let N and L be 18 and 48, respectively. For VQE, θ_l^i 's are firstly sampled from 0 to 2π uniformly as the starting point, and $\theta \in \mathbb{R}^{12,240}$ is then updated iteratively to min-

imize $h(\theta)$. After repeating this optimization process 10 times, the mean value of the average energy after 1,000 iterations is found to be only -0.1367. Since the exact average ground energy is -1.7828, such a poor result indicates the strong impact of BPs.

When it turns to the VQE-SA method, a θ is initialized uniformly from $\{\theta_l^i \in [0, 0.01]\}$ as the starting point, and then it is updated iteratively to search for the ground state. As for VGON, 8,000 θ 's are uniformly initialized from $\{\theta_l^i \in [0, 2\pi]\}$ as the inputs of the model, which contains a 7-layer encoder network with sizes [8192, 4096, 2048, 1024, 512, 256, 128], a latent space with dimension 100, and a 7-layer decoder network with sizes [128, 256, 512, 1024, 2048, 4096, 8192]. Set the batch size to 8, and the coefficient of the KL divergence to 0.1. We run both of the two methods for 1,000 iterations with all the other configurations kept the same as VQE. To make a fair comparison, we repeat the whole process 10 times. Fig. 3 in the main text illustrates the corresponding mean values and the 95% confidence intervals of the energy densities and the fidelities between the optimized state and the ground state at different iterations, where we can clearly see the faster and more stable convergence of VGON than the VQE-SA method.

Appendix D: Identifying degenerate ground state space of quantum models

As evidenced earlier, the VGON model exhibits excellent capabilities in solving optimization problems with a single optimal solution. In this section, by solving a degenerate ground space we demonstrate that VGON also has the capability to effectively handle optimization problems with multiple optimal solutions.

To identify the degenerate ground space of a Hamiltonian H with VGON, the objective function needs two pivotal components to steer the optimized quantum state $|\psi(\theta)\rangle$ towards diverse ground states. The first component utilizes a PQC $U(\theta)$ to generate the state $|\psi(\theta)\rangle = U(\theta)|00\dots 0\rangle$, targeting the ground space. The second component integrates a cosine similarity measure into the optimization objective, aiming to enhance the diversity among the generated quantum states.

Specifically, for a batch of S_b states $\{|\psi(\theta_i)\rangle\}$, the mean energy is calculated by

$$\bar{E}(\Theta) = \frac{1}{S_b} \sum_{i=1}^{S_b} \langle \psi(\theta_i) | H | \psi(\theta_i) \rangle,$$

where $\Theta = (\theta_1, \theta_2, \dots, \theta_{S_b})$. In addition, a penalty term for the objective function based on the cosine similarity is defined as

$$\bar{S}_{C_{S_b}^2}(\Theta) = \frac{1}{|C_{S_b}^2|} \sum_{(i,j) \in C_{S_b}^2} \frac{\theta_i \cdot \theta_j}{\|\theta_i\| \|\theta_j\|},$$

where $C_{S_b}^2$ represents the set of all 2-combinations pairs derived from the elements in $\{1, 2, \dots, S_b\}$, and $\|\cdot\|$ denotes the Euclidean norm. Eventually, the optimization objective is set as minimizing of a combination of $\bar{E}(\Theta)$ and $\bar{S}_{C_{S_b}^2}(\Theta)$ according to a trade-off coefficient γ , i.e.,

- **Objective function:** $h(\Theta) = \bar{E}(\Theta) + \gamma \cdot \bar{S}_{C_{S_b}^2}(\Theta)$
- **Parameter space:** $\{\Theta \in \mathbb{R}^{S_b M}\}$

In this section, we consider the ansatz expressed by Eq. (C1), hence M equals $15(N-1)L$, where N and L are the number of qubits and layers in the circuit, respectively.

1. The Majumdar-Ghosh model

The Majumdar-Ghosh (MG) model, a one-dimensional chain of interacting spins with next-nearest-neighbor interactions, is a classic example exhibiting substantial degeneracy under open boundary conditions, whose Hamiltonian is written as

$$H_{MG} = \sum_{i=1}^N \sigma_x^i \cdot \sigma_x^{i+1} + \sigma_x^{i+1} \cdot \sigma_x^{i+2} + \sigma_z^i \cdot \sigma_z^{i+2},$$

where $\sigma^i = (\sigma_x^i, \sigma_y^i, \sigma_z^i)$ are Pauli operators at site i . In the MG model, the local 3-site term is a sum of 2-local swap operations, resulting in a 4-dimensional ground antisymmetric space. As the particle number grows, the ground space is determined by intersecting the added state space with the previous ground space, with dimensions of 4 for odd sizes and 5 for even sizes.

For the case that $N = 10$, whose exact ground energy is -24, we set $L = 4$, resulting in 36 universal 2-qubit gate blocks, and the batch size $S_b = 50$. To balance the diversification of generated states with their eventual convergence to the ground space, the trade-off coefficient γ is dynamically adjusted across different iterations using a step function that gradually decreases from 40 to 1.

The VGON model employed to tackle this task has a 4-layer encoder network with sizes [512, 256, 128, 64], a latent space with dimension [50], and a 4-layer decoder network with sizes [64, 128, 256, 512]. During the training procedure, a dataset randomly sampled from a uniform distribution on the interval $[0, 1]$ is utilized. The hyperparameter β serving as the coefficient of the KL divergence and the learning rate are set as 1 and 0.0014, respectively. The training is terminated upon reaching an energy value of -23.90.

Among the 1000 generated states, 81.9% achieve the energy threshold of -23.90. To examine the diversity of the generated states, we analyze the overlaps between the states achieving the above threshold and all the ground states, as shown in Fig. 11. It can be clearly seen that the generated states exhibit significant diversity. To ensure that VGON's outputs effectively involve all the dimensions of the

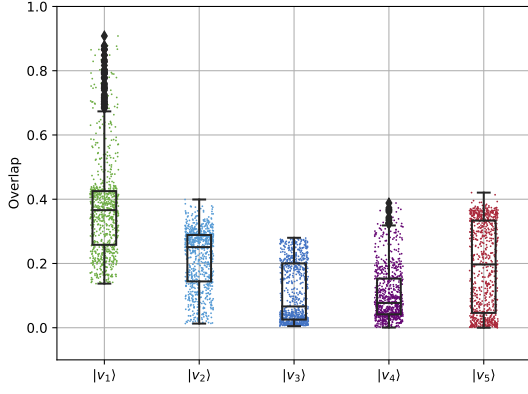


FIG. 11 The overlaps between the generated states of VGON and the ground states. Each boxplot shows the degree of dispersion and skewness for the overlap with one ground state. Table III lists the minimum, lower quartile, median, upper quartile, and maximum for each ground state.

TABLE III Details on the overlap boxes of VGON's output on the basis of the degenerate space of H_{MG} .

Basis	Minimum	Lower Quartile	Median	Upper Quartile	Maximum
$ v_1\rangle$	0.1373	0.2581	0.3660	0.4252	0.9081
$ v_2\rangle$	0.0129	0.1442	0.2509	0.2887	0.3992
$ v_3\rangle$	0.0050	0.0254	0.0663	0.2002	0.2800
$ v_4\rangle$	0.0007	0.0418	0.0772	0.1529	0.3882
$ v_5\rangle$	0.0001	0.0463	0.1969	0.3335	0.4206

ground space, we set the overlap threshold to 0.001 and then analyze all the generated states. The results indicate that 81.4% of the generated states meet both the energy and the overlap thresholds. Fig. 12 exhibits ten such generated states, which not only illustrates the remarkable diversity of the solutions provided by VGON, but also demonstrates VGON's capability of identifying degenerate ground state spaces for quantum models effectively.

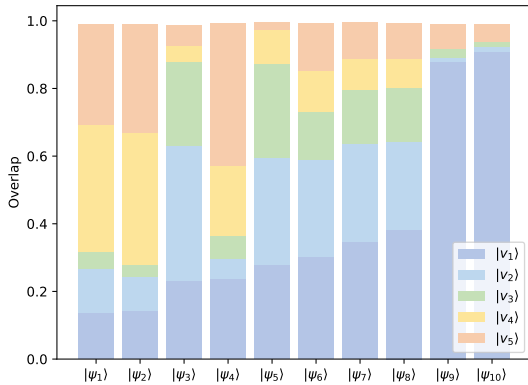


FIG. 12 The overlaps between selected generated states and the degenerate space. Five bases of the degenerate space, represented by $|v_1\rangle - |v_5\rangle$, are determined through the exact diagonalization method. For each generated state $|\psi_i\rangle$, the corresponding bars with different colors represent the overlaps into different bases.

2. The 232 model

In this context, a model that exhibits a degeneracy of 2 for odd sites with open boundary conditions is considered, whose Hamiltonian is (Yang *et al.*, 2022)

$$H_{232} = \sum_{i=1}^N (2\sigma_x^i \sigma_x^{i+1} + \sigma_x^i \sigma_y^{i+1} - \sigma_y^i \sigma_x^{i+1}),$$

where $\sigma_{x,y,z}^i$ represent the Pauli matrices at site i . Let the number of qubits N be 11, the corresponding ground energy is -20.7106 .

Consider $L = 6$, resulting in the number of universal 2-qubit gate blocks being 60, and the batch size $S_b = 50$. The configurations of the VGON model and the training procedure remain consistent with that in Appendix D.1, except for setting the learning rate to 0.0015 and terminating the training upon reaching an energy value of -20.6106 .

After training, 1,000 quantum states are generated by the VGON model, with 78.7% demonstrating energies below -20.6106 . As illustrated in Fig. 13(a), the overlap distribution on each basis state, denoted as $\{|u_1\rangle, |u_2\rangle\}$, showcases a bimodal pattern, precisely reflecting the degree of degeneracy. Moreover, the analysis of fidelities between pairs of generated states, depicted in Fig. 13(b), reveals values clustering around either 0 or 1. This indicates that the states generated by the VGON model are either identical or orthogonal to each other. Consequently, this affirms VGONs' capability to directly generate a complete set of orthogonal bases for this task.

TABLE IV Boxplot details on overlap distributions for the basis of the degenerate space of H_{232} , and the distributions of fidelities between pairs of generated states.

	Minimum	Lower Quartile	Median	Upper Quartile	Maximum
$ u_1\rangle$	0.1895	0.2063	0.6564	0.65820	0.6608
$ u_2\rangle$	0.1873	0.1907	0.1913	0.6777	0.6845
Fidelity	2.7511×10^{-15}	4.8752×10^{-9}	0.9882	0.9978	0.9998

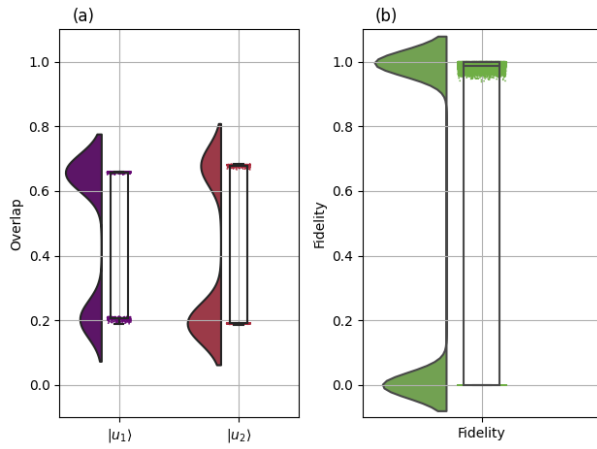


FIG. 13 Distributions of the generated states for the 232-type model. (a) The overlap distributions for the basis states $|u_1\rangle$ and $|u_2\rangle$, whose population densities plots are both bimodal, consistent with the degree of degeneracy. The minimum, lower quartile, median, upper quartile, and maximum for each basis state are presented in the first part of Table IV. (b) The distribution of fidelities between pairs of generated states with energies below -20.6106. The population densities plot reveals a bimodal distribution, with pronounced peaks near 0 and 1. This pattern suggests that the states are predominantly either identical (fidelity close to 1) or orthogonal (fidelity close to 0) to each other. The statistical summary of the boxplot is shown in the second part of Table IV.